KEK Preprint 95-154
November 1995
H/D

Performance Simulation of Liquid Xenon Ionization Drift Chamber for Detecting Double Beta Decay of ^{136}Xe

H. TAWARA, M. MIYAJIMA, S. SASAKI
and
A.G. PROKOPETS

Submitted to the Fifth EGS4 Users' Meeting in Japan,
KEK, Tsukuba, Japan, July 23 - 25, 1995.

National Laboratory for High Energy Physics, 1995

KEK Reports are available from:

Technical Information & Library
National Laboratory for High Energy Physics
1-1 Oho, Tsukuba-shi
Ibaraki-ken, 305
JAPAN

Phone: 0298-64-1171
Telex: 3652-534 (Domestic)
(0)3652-534 (International)
Fax: 0298-64-4604
Cable: KEK OHO
E-mail: LIBRARY@JPNKEKVX (Bitnet Address)
library@kekvax.kek.jp (Internet Address)

Performance Simulation of Liquid Xenon Ionization Drift Chamber for Detecting Double Beta Decay of ^{136}Xe

H. Tawara, M. Miyajima and S. Sasaki

National Laboratory for High Energy Physics, 1-1 Oho, Tsukuba-shi, Ibaraki-ken, 305, Japan

A. G. Prokopets

The Graduate University for Advanced Studies, 1-1 Oho, Tsukuba-shi, Ibaraki-ken, 305, Japan

(November 15, 1995)

Abstract

An EGS4/PRESTA [1,2] user code, UCLXE.MOR, is now being developed to simulate the performance of a liquid xenon ionization drift chamber (LXeIDC) for detecting the neutrinoless double beta ($0\nu\beta\beta$) decay of ^{136}Xe. The initial results of a Monte Carlo calculation are reported here. The "detector efficiency" of $0\nu\beta\beta$ decay events was computed to be 85% for a prototype detector with a 1 liter active volume. The trajectories of β-rays on the $0\nu\beta\beta$ decay event, as well as the 2.6-MeV gamma-ray from ^{208}Tl, which is expected to be a dominant background source in an ^{136}Xe $0\nu\beta\beta$ decay experiment, were calculated in order to develop various discrimination algorithms for improving the background-reduction capability of the detector.

I. INTRODUCTION

A nuclear double beta ($\beta\beta$) decay [3] experiment has been an extremely attractive attempt, because it may probe grand unification scales far beyond the present and future accelerator energies [4]. The neutrinoless double beta ($0\nu\beta\beta$) decay is one of the $\beta\beta$ decay modes which have been predicted theoretically. It is a lepton non-conserving process, and is

forbidden in the Standard Model. This decay mode can take place only when the electron neutrino is a massive Majorana particle [5–7]. The neutrino mass plays a key role in modern theoretical particle physics, and is one of the candidates for non-baryonic dark matter in the universe. The observation of $0\nu\beta\beta$ decay also provides information concerning the structure of weak interactions, such as leptonic currents with a small right-handed component.

The Q value, i.e., the kinetic energy available to the leptons, is shared by two electrons in the case of the $0\nu\beta\beta$ $[0^+ \rightarrow 0^+]$ transition of the two-nucleon mechanism; consequently, the sum-energy spectra of the two electrons exhibits a monochromatic peak at the Q value, as illustrated in fig.1. The $0\nu\beta\beta$ decay may take place via other possible non-nucleonic mechanisms, such as a process involving the emission of a Majoron (X) [8,9]. As shown in fig.1, the $0\nu,X\beta\beta$ mode displays a typical three-body decay spectrum peaked at approximately 80% of the Q value. On the other hand, the $2\nu\beta\beta$ mode shows a four-body decay spectrum peaked at around 40% of the Q value. The energies carried by the residual nucleus in the $\beta\beta$ decay modes are negligible.

We have developed a self-triggered liquid xenon ionization drift chamber with a multi-segmented collector electrode for the ^{136}Xe $0\nu\beta\beta$ decay experiment [10,11]. Liquid xenon is one of the prominent materials for the $\beta\beta$ decay experiment. Nuclear energy level schemes for ^{134}Xe and ^{136}Xe are shown in fig.2. Since the Q value of ^{136}Xe(2.479 MeV) is large compared to that of other candidate isotopes, a shorter half-life can be expected, because the decay rate is proportional to the phase space, which is proportional to some powers of the Q value. Furthermore, the background rate, such as that of gamma-rays due to natural radioactive isotopes, drops exponentially toward the higher energy region. Liquid xenon is advantageous not only as a source of $\beta\beta$ decay (^{134}Xe,^{136}Xe), but also as a medium for a radiation detector, as described in the section II.

However, the observation of $\beta\beta$ decays is extremely complicated because of their long half-lives. Recently, the Gotthard group has reported the following 90% C.L. half-life limits for the $[0^+ \rightarrow 0^+]$ transition: 0.37×10^{24} years in the "mass mechanism" mode, and 0.28×10^{24} years in the "right-handed weak currents" mode [12]. Their enriched gaseous xenon TPC

has around a 30% "detector efficiency", i.e., the probability that the kinetic energies of two electrons from $\beta\beta$ decay are completely deposited in the active volume [13]. There has been, however, no obvious evidence of $0\nu\beta\beta$ decay up to the present in any existing experiment. Any future progress in the search for $\beta\beta$ decay strongly depends on further improvements of the signal-to-background ratio. The use of liquid xenon allows us to increase the detection efficiency as well as the number of candidate isotopes. Furthermore, massive liquid xenon, itself, is an effective shielding material to background, especially alpha particles or "single" beta-rays emitted from radioactive isotopes included in the internal components of a detector. The higher sensitivity in the $\beta\beta$ decay experiment can, therefore, be achievable even after applying a background-rejection method, such as a "fiducial volume cut" and a signal analysis.

It is troublesome to experimentally assess the detector performance, such as the detection efficiency and the capability of background reduction in the $\beta\beta$ decay experiment. The Monte Carlo electron-photon transport code with a Parameter Reduced Electron-Step Transport Algorithm, EGS4/PRESTA [1,2], is useful to simulate physical processes caused by beta-ray and gamma-ray in liquid xenon. We are now developing the EGS4/PRESTA user code, UCLXE.MOR, in order to obtain information about the performance of a liquid xenon ionization drift chamber (LXeIDC) for $\beta\beta$ decay experiments.

We report here on some preliminary results concerning a calculation using UCLXE.MOR for the ^{136}Xe $0\nu\beta\beta$ decay experiment with the prototype detector: the detector efficiency, expected spectra of the $\beta\beta$ decay event, as well as background gamma-ray from ^{208}Tl which is the most probable background source under typical laboratory conditions. In addition, the trajectories of $0\nu\beta\beta$ decay events and gamma-ray events have been discussed in order to develop the method for rejecting background signals by analysing charge signals from a multi-segmented collector electrode.

II. LIQUID XENON IONIZATION DRIFT CHAMBER

The prototype LXeIDC has been constructed at the National Laboratory for High Energy Physics (KEK). The superior properties of a liquid xenon detector for beta-ray and gamma-ray spectroscopy, namely for the $\beta\beta$ experiment, are the following. The small W-value (15.6 eV) [14], the low diffusion coefficient (65 cm^2s^{-1}) [15] and the large drift velocity (3×10^5 cms^{-1} at >3 kV/cm) [16,17] for free electrons are good for an ionization chamber. The high yield ($> 1.5 \times 10^5$ photons at 2.5 MeV) [18,19] and the fast decay (fast component, 3 ns) [20] of scintillation light provide an excellent scintillation detector with the fast triggering capability. The high density (3.06 gcm^{-3} at -109 °C), high atomic number (Z=54), nearly constant drift velocity above the 5 kV/cm electric field and the flexibility of liquid allow a large-size position sensitive detector with an excellent detection efficiency.

Figure 3 is a cross-sectional view of the main part of apparatus. The prototype is a single gridded ionization chamber and a scintillation detector equipped with four photomultipliers. The detector system has been reported in detail [10,11].

The detector has a cylindrical active volume of 1 liter between the cathode and the grid plane. The length of the drift region is 4 cm. This kind of long-distance drift of free electrons can be achievable only in very high-purity liquid xenon, which is obtained by using a rare-gas purification system [21]. The natural abundance of ^{136}Xe is 8.87%, giving a total of 1.2×10^{24} ^{136}Xe atoms in the active volume. The use of liquid xenon enriched up to 100% of ^{136}Xe provides candidate atoms of 1.3×10^{25}, which is equivalent to that of the enriched gaseous TPC in the Gotthard experiment [12,13]. One of the unique properties of the detector is the multi-segmented collector electrode(fig.4). It contains 37 hexagonal segments with a side length of 14.5 mm and 6 irregular shape ones. This multi-segmented structure of the collector electrode allows the LXeIDC to work as an association of 43 "small ionization chambers", thus, the energy measurement for each event is performed on those chambers independently due to the detected charge. The acquisition of charge signals from segments is triggered by corresponding scintillation light. The position of a segment with a charge

signal provides spatial information concerning the energy deposition on the X-Y plane. The time evolution of a charge signal also gives information along the Z-direction.

This collector structure is intended to use an anti-coincidence method to identify background signals, as discussed in the following section.

III. MONTE CARLO CALCULATION

A. Model of LXeIDC

Figure 5 illustrates the model of the LXeIDC simplified for Monte Carlo calculations. It comprises two materials for an initial examination: vacuum and liquid xenon, with a density of 3.06 gcm^{-3}. The liquid xenon region is divided into two regions: an active volume (drift region) and a dead volume enveloping the active volume. This geometry can be described by a combination of two coaxial cylinders and five parallel planes, which are coded by using the geometry Macros in EGS4 code. In the EGS4/PRESTA calculation, UCLXE.MOR scores the energy deposition and the X-, Y-, Z-coordinates of every step in the history of particle transportation, and then determines the position of the segments including that scored point.

B. Source

The following two kinds of sources were used in the calculation:

a. $0\nu\beta\beta$ decay: The source to be distributed uniformly in a liquid xenon region is assumed. At any source, two electrons are generated and go to the opposite direction of each other. Although the Q value of decay(2.479 MeV) is shared by these electrons, the ratio of kinetic energies carried by them is selected at random.

b. Background: The pulse-height spectrum of background measured by a $2''\phi \times 2''$ NaI(Tl) scintillator in a concrete building is shown in fig.6 [22]. It is indicated that the dominant background superimposed on the peak of $0\nu\beta\beta$ decay is gamma-rays from ^{208}Tl.

For the first demonstration, 2.6MeV gamma-rays isotropically incident on the surface of the liquid xenon region from outside was assumed as a background source. The uniformity of the flux of gamma-ray was assured over the liquid xenon region.

IV. RESULTS AND DISCUSSION

A. Energy Spectra and Detector Efficiency

The spectra of $0\nu\beta\beta$ decay and gamma-rays from the LXeIDC have been calculated as shown in fig.7. It was assumed that the energy resolution is 3.5% in FWHM at 2.5 MeV and is inversely proportional to the square root of energy [23]. These spectrum predict that the peak of the $0\nu\beta\beta$ decay event is situated in the trough between the Compton edge and the full-energy peak of 2.6 MeV gamma-rays. The signal-to-background ratio strongly depends on the energy resolution. A further calculation of the energy resolution dependence is now being performed with a background-rejection algorithm, as discussed in the following sections.

In the gamma-ray spectrum, single- and double-escape peaks are evident. The existence of liquid xenon in a dead volume contributes to create a peak at 511 keV due to annihilation photons and a backscatter peak at around 250 keV due to Compton scattering.

The 3σ detector efficiencies were obtained to be 85% for a 1-liter active volume, and 53% for a small chamber, which is segmented with about a 5.4 cm^3 volume, respectively. The liquid xenon chamber displays an extremely high detection efficiency which is comparable to that of the Ge detector (about 90%) for the $\beta\beta$ decay experiment [24].

B. Anti-coincidence Method using a Multi-segmented Collector

A simulation of the spatial distribution of the energy deposition in liquid xenon due to beta-rays and gamma-rays is quite helpful not only for estimating the detection efficiency, but also for demonstrating of charge and scintillation signals in order to develop various

discrimination algorithms which can reject background signals in an on-line analysis, as well as in an off-line one.

A $\beta\beta$ decay event in liquid xenon is observed as a continuous energy deposition, that is, a "single-site charge-blob" the size of which is typically about 2 mm. On the other hand, the interaction of gamma-rays in liquid xenon (Z=54) is dominated by Compton scattering in the energy region from 300 keV to 6 MeV (see fig.8 taken from The Atomic Nucleus by R. D. Evans [25]). Therefore, gamma-rays in the MeV energy region mainly give rise to Compton scattering, which generates a multiple-scattered energy deposition, that is, "multi-site charge-blob", in liquid xenon. Figures 9a and 9b show the trajectories on an X-Y plane of beta-rays emitted from ^{136}Xe (a), and of 2.6 MeV gamma-rays (b) displayed by using the EGS4 shower display system (EGS4PICT) [26]. The inside of the inner circle corresponds to an active volume of 1 liter.

The solid lines shown in fig.10 demonstrate the energy depositions on $0\nu\beta\beta$ decay events (a, b) and gamma-ray events (c) along the Z-direction in seven neighboring segmented drift regions, respectively. The single-site charge-blobs due to beta-rays mostly generate a charge signal from only one segment (fig.10a), or those from two neighboring segments which appear at the same time (fig.10b). Although a coincidence of signals from three neighboring segments is also possible, the fraction is quite small. The multi-site charge-blobs of gamma-rays can generate plural charge signals from more than three segments, or those not from neighboring segments (fig10c). It is also possible that an anti-coincidence in time occurs among them. Accordingly, some of the multiple-Compton scattering events can be distinguished from the $\beta\beta$ decay events by means of an anti-coincidence method using a multi-segmented collector. The rejection efficiency of 2.6 MeV gamma-ray events from the 3σ interval of the $0\nu\beta\beta$ peak is roughly 30% with the present structure of the multi-segmented collector. This efficiency depends on the size of a segment. Although the smaller segment size might be desirable, it would leads to an increase in the number of electronic parts.

C. Pulse Shape Analysis

In addition to the anti-coincidence method mentioned above, the pulse shapes of charge signals from segments offer information along the Z-direction which can be used to identify gamma-ray events, even when a gamma-ray deposits its entire energy into one or two neighboring segments.

The charge-blobs of a gamma-ray event, which are superimposed on the $0\nu\beta\beta$ decay peak, splash along the Z-direction up to 4 cm long, as shown in fig.11a. This length is equivalent to those of the drift region. On the other hand, the $\beta\beta$ decay events are put in a compact space (fig.11b). The shapes of the integrated energy deposition (the broken lines in fig.10) reflect the time evolution of the charge signal (typically on the rise time). The rise time of pulses from segments correspondent with the $\beta\beta$ event is shorter than those due to gamma-rays in many cases. For a more precise analysis of the pulse shape, it is necessary to take into consideration the drift time between the grid-collector region, the distribution of charges along the Z-direction, the effect of the shielding inefficiency of the grid electrode, and the diffusion of electrons.

V. CONCLUSION

A monte Carlo calculation predicts that an LXeIDC with a multi-segmented collector electrode has an excellent detection ability of the $\beta\beta$ decay event. The EGS4/PRESTA code can produce the useful information for the anti-coincidence method and for the pulse-shape analysis intended to reject background. The anti-coincidence capability of the LXeIDC associated with a properly designed multi-segmented collector can be expected to greatly improve the signal-to- background ratio.

The results of a Monte Carlo calculation, such as the detection efficiency, should be assessed more carefully because many simplifications, for example, a geometry model of a detector, could cause a large ambiguity [27]. In addition to ^{208}Tl, the background from

other natural radioactive isotopes, cosmic rays, activation of instrument materials must be taken into account. A precise pulse shape analysis of the charge signals associated with scintillation signals is also needed.

A simulation of the $2\nu\beta\beta$ decay experiment is being planed. The user code UCLXE.MOR is intended to be continuously improved along with the advancement of the experiment.

REFERENCES

[1] W. R. Nelson, H. Hirayama, and D. W. O. Rogers, SLAC-265 (Stanford University, Stanford 1985).

[2] A. F. Bielajew, and D. W. O. Rogers, Nucl. Instrum. and Meth. **B18**, 165 (1987).

[3] F. Boehm and P. Vogel, "Physics of Massive Neutrinos", 2nd ed., Cambridge University Press, Cambridge, England (1992).

[4] H. V. Klapdor-Kleingrothaus and A. Staudt, "Non-Accelerator Particle Physics", A. Hilger, Bristol, New York (1994).

[5] J. Schechter and J. W. F. Valle, Phys. Rev. **D25**, 2951 (1982).

[6] J. F. Nieves, Phys. Lett. **147B**, 375 (1984).

[7] E. Takasugi, Phys. Lett. **149B**, 372 (1984).

[8] G. B Gelmini, S. Nussinov, and M. Roncadelli, Nucl. Phys. **B209**, 157 (1982).

[9] H. M. Georgi, S. L. Glashow, and S. Nussinov, Nucl. Phys. **B193**, 297 (1981).

[10] A. G. Prokopets et al., KEK Proceedings **94-7**, 60 (1994).

[11] A. G. Prokopets et al., KEK Proceedings **95-1**, 183 (1995).

[12] V. Jörgens et al., Nucl. Phys. **B35**, 378 (1994).

[13] J. -C. Vuilleumier et al., Phys. Rev. **D48**, 1009 (1993).

[14] T. Takahashi et al., Phys. Rev. **A12**, 1771 (1975).

[15] E. Shibamura et al., Phys. Rev. **A20**, 2547 (1979).

[16] L. S. Miller, S. Howe, and W. E. Spear, Phys. Rev. **116**, 871 (1968).

[17] E. Shibamura et al., Nucl. Instr. and Meth. **131**, 249 (1975).

[18] M. Miyajima et al., IEEE Trans. Nucl. Silence, **NS39**, 536 (1992).

[19] T. Doke, K. Masuda, and E. Shibamura, Nucl. Instr. and Meth. **A291**, 617 (1990).

[20] S. Kubota et al., Nucl. Instr. and Meth. **196**, 101 (1982); S. Kubota et al., Nucl. Instr. and Meth. **A242**, 291 (1986); S. Kubota, M. Hishida, and J. Raun (Gen), J. Phys. **C11**, 2645 (1978).

[21] M. Miyajima et al., Nucl. Instr. and Meth. **134**, 403 (1976).

[22] M. Miyajima, Hoshasen, **15-1**, 45 (1988), in Japanese.

[23] E. Aprile, R. Mukherjee and M. Suzuki, Nucl. Instr. and Meth. **A302**, 177 (1991).

[24] F. Petry et al., Nucl. Instr. and Meth. **A332**, 107 (1993).

[25] R. D. Evans, "The Atomic Nucleus", MacGrow-Hill (1955).

[26] H. Hirayama et al., KEK Internal **94-10** (1994).

[27] H. S. Miley et al., Nucl. Phys. **B35**, 388 (1994).

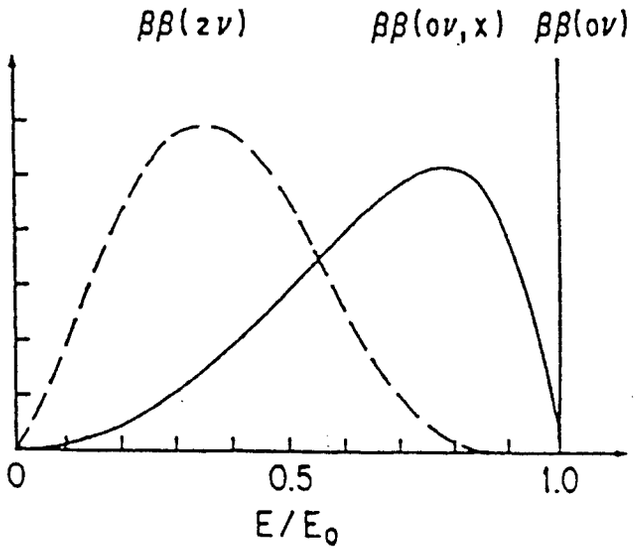

FIG. 1. Theoretically predicted sum-energy spectra of the two electrons emitted in the following decay modes: 2ν mode : $(A,Z) \rightarrow (A,Z+2) + 2e^- + 2\bar{\nu}$, 0ν mode : $(A,Z) \rightarrow (A,Z+2) + 2e^-$, and 0ν,X mode : $(A,Z) \rightarrow (A,Z+2) + 2e^- + X$.

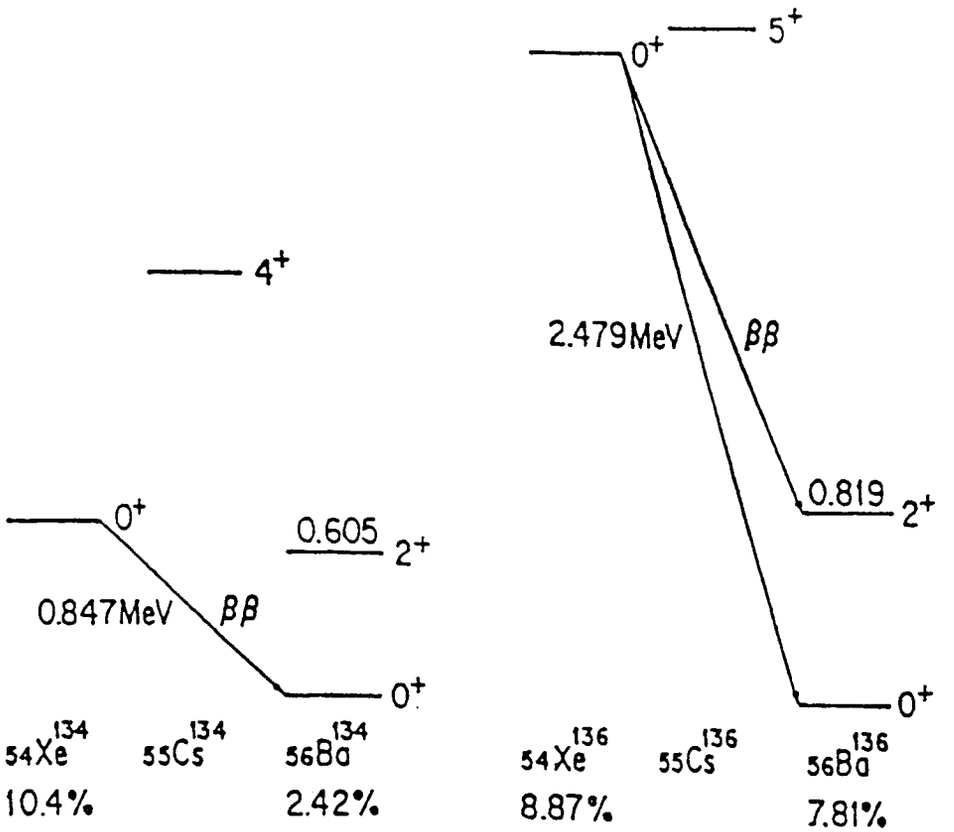

FIG. 2. Nuclear energy level schemes of ^{134}Xe, ^{136}Xe on $\beta\beta$ decay. The natural isotopic abundances are shown below the isotopes concerning the decay.

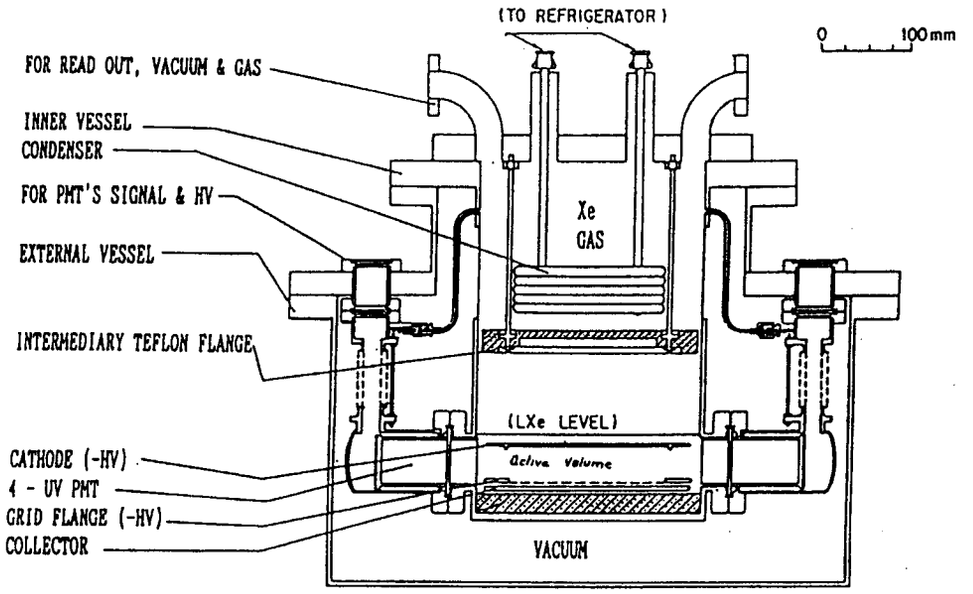

FIG. 3. Cross-sectional view of the self-triggered liquid xenon ionization drift chamber.

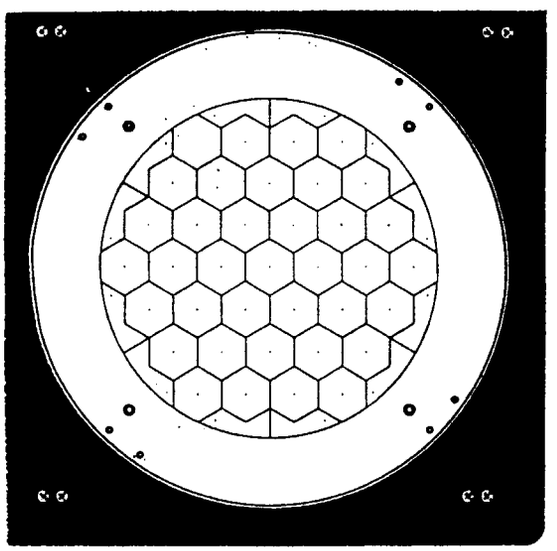

FIG. 4. Multi-segmented collector of the prototype detector.

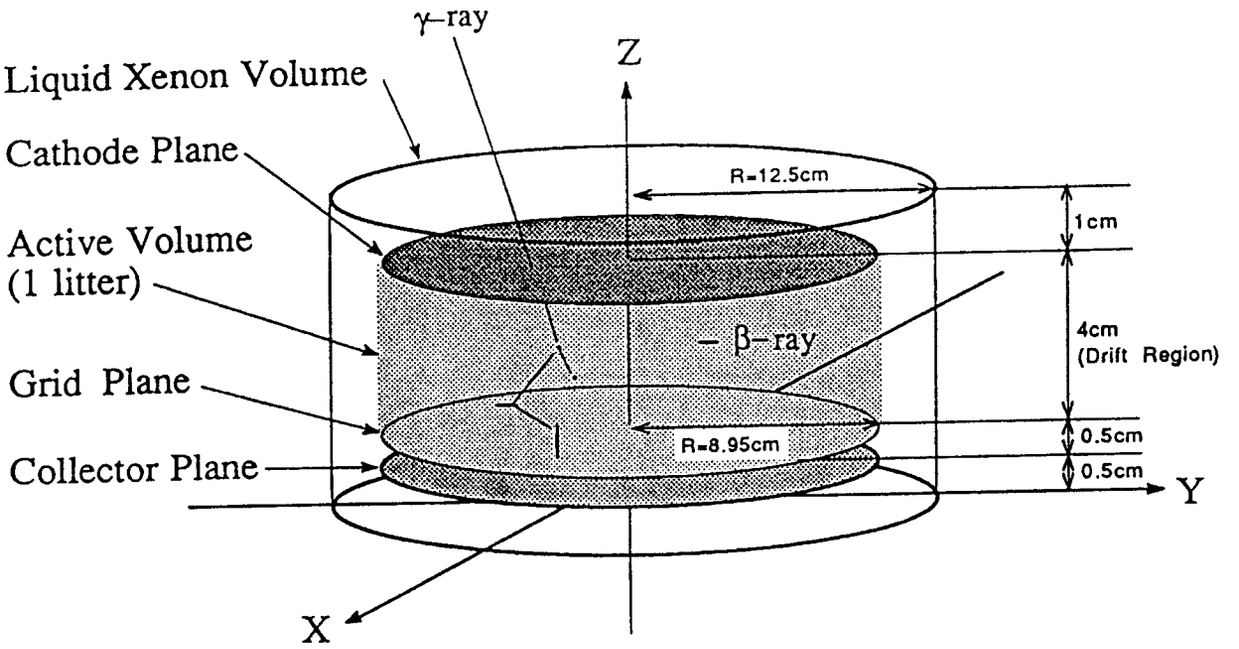

FIG. 5. Simplified model of LXeIDC for an EGS4/PRESTA Monte Carlo calculation.

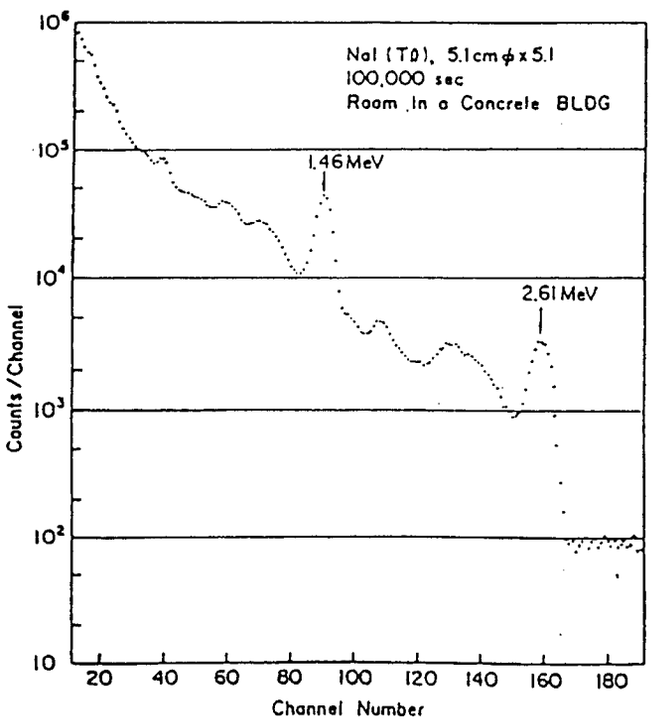

FIG. 6. Pulse-height spectrum of the background measured by a $2''\phi \times 2''$ NaI(Tl) scintillator in a concrete building.

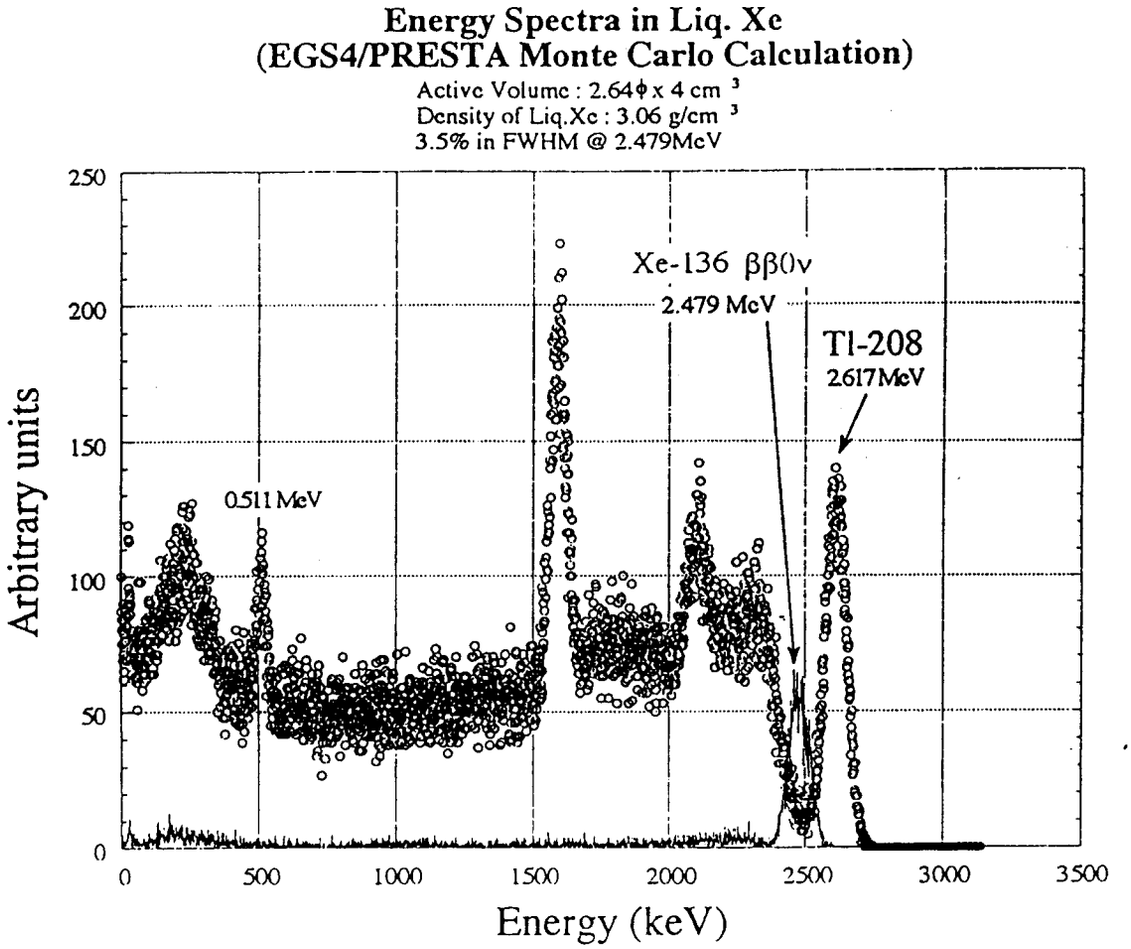

FIG. 7. Simulated spectra of ^{136}Xe $0\nu\beta\beta$ decay (solid line) and of 2.6 MeV gamma-ray (circles) from LXeIDC. The density of liquid xenon is assumed to be 3.06 gcm^{-3}.

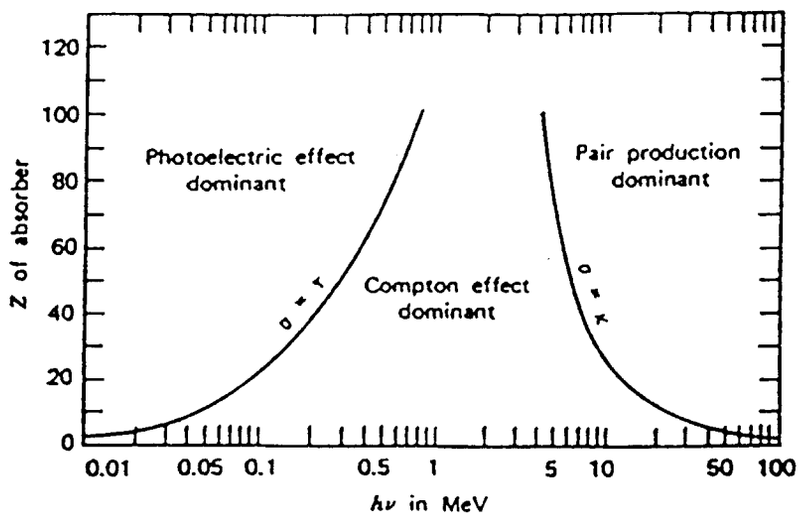

FIG. 8. Relative importance of the three principal types of gamma-ray interactions in matter (From The Atomic Nucleus by R. D. Evans).

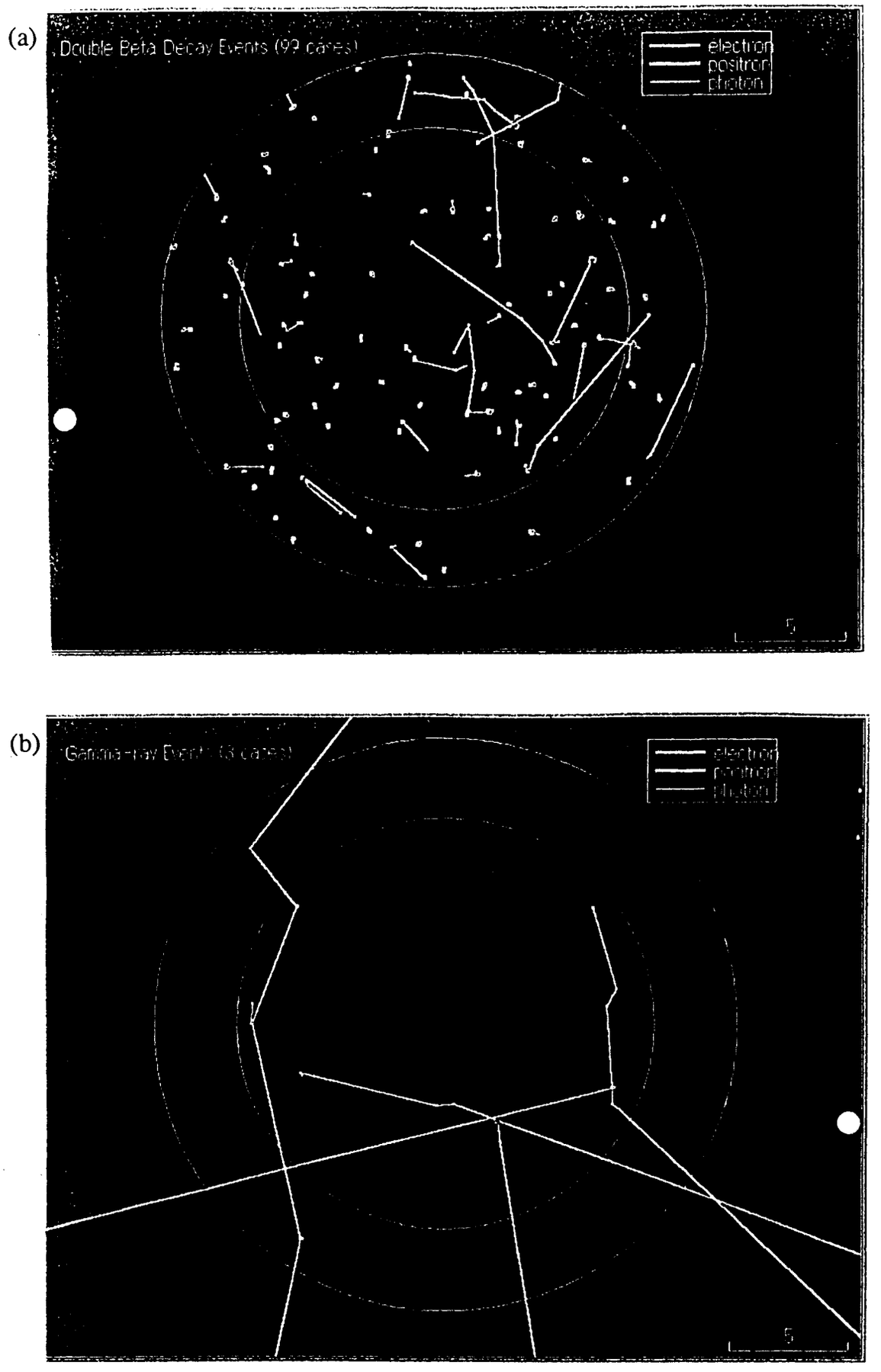

FIG. 9. Simulation of the particle trajectories of electrons from $0\nu\beta\beta$ decay (a) and of 2.6 MeV gamma-rays (b). The X-Y projection are shown. The unit of scale on the right bottom is in cm.

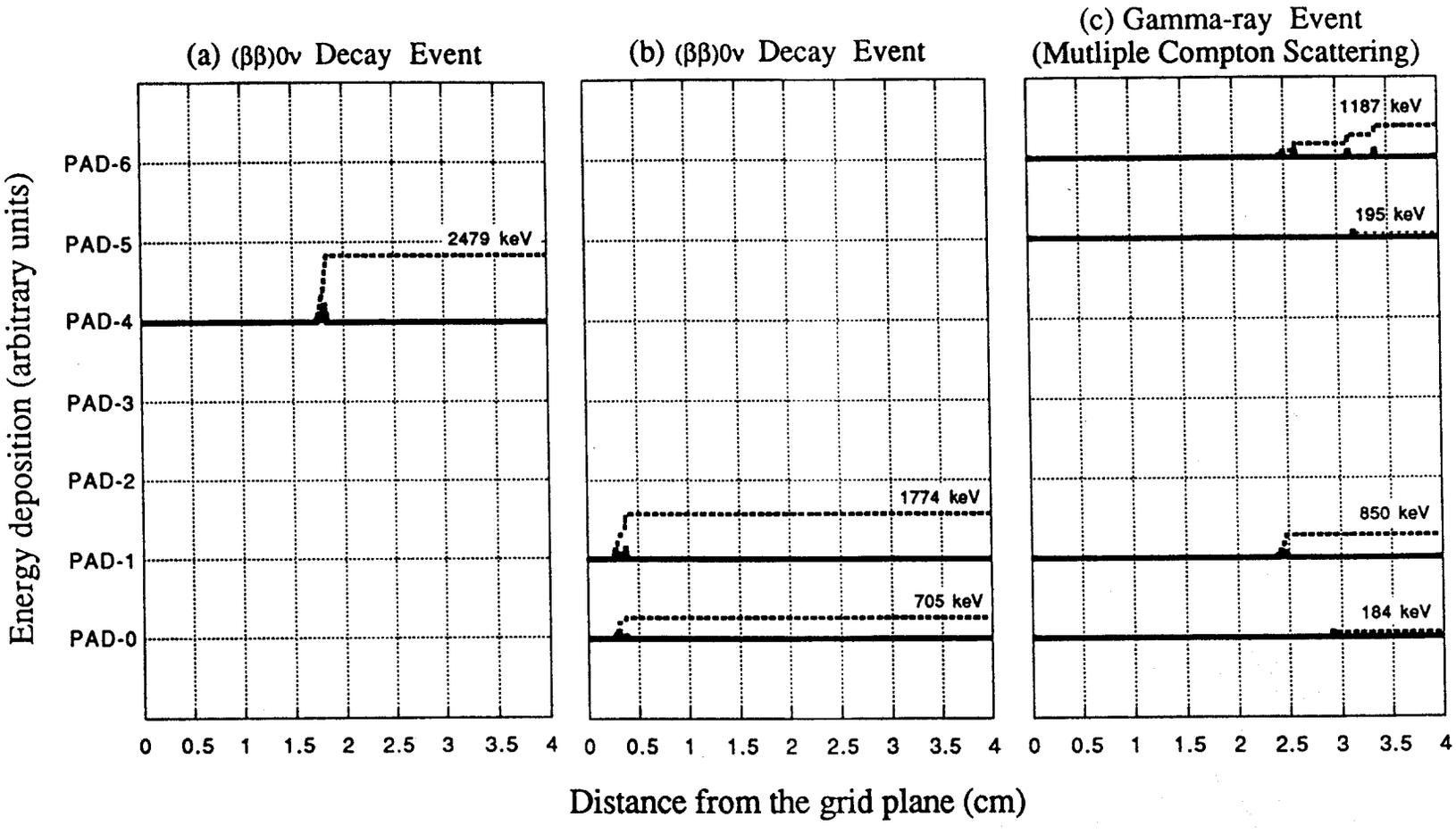

FIG. 10. Examples of the calculated energy depositions in seven neighboring segmented drift regions (pad-0 to pad-6) due to $0\nu\beta\beta$ decay (a,b) and 2.6 MeV gamma-ray (c). Solid and broken lines indicate the energy depositions and the integrated ones along the Z-direction, respectively.

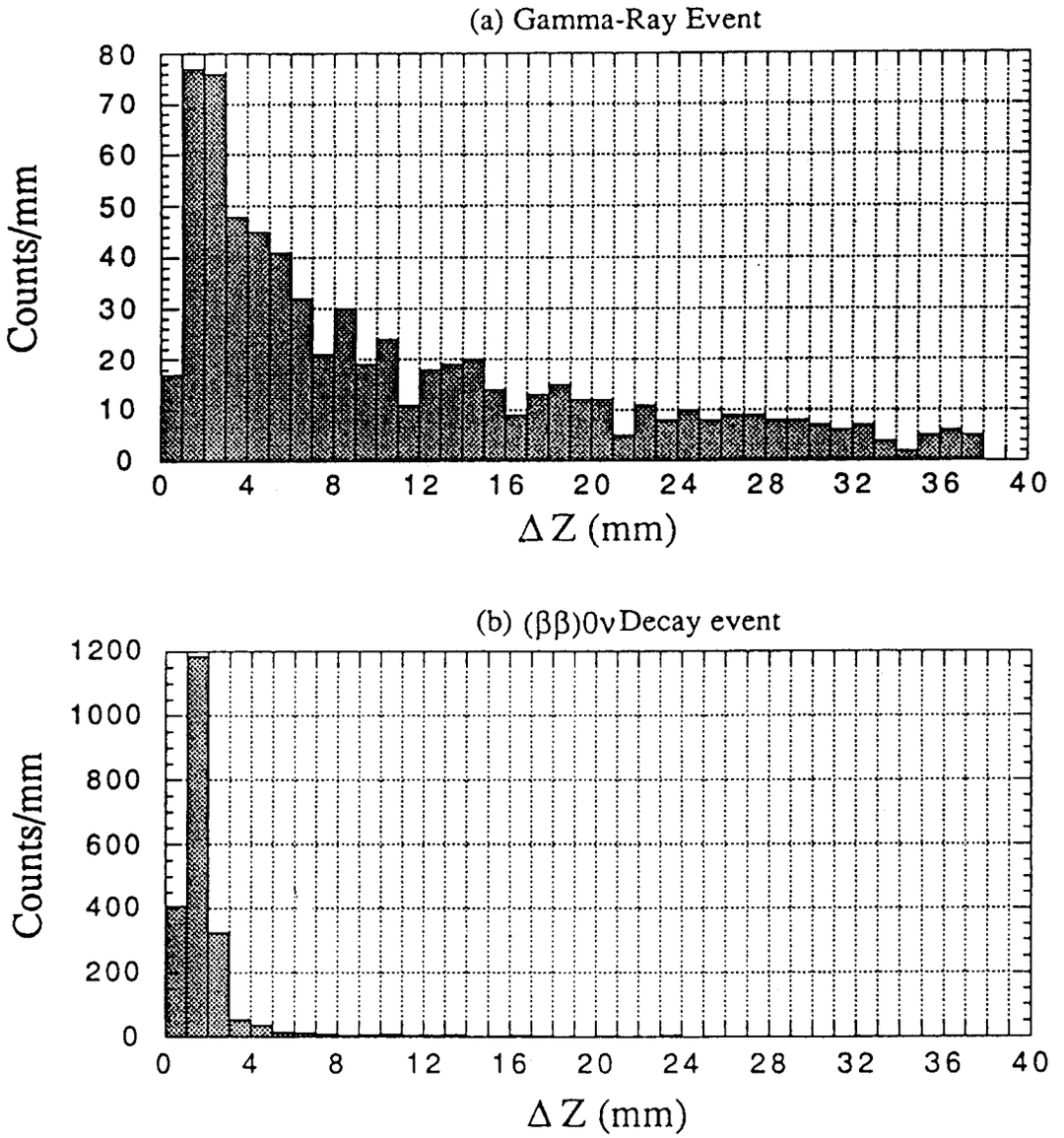

FIG. 11. Distribution of the interval along Z-direction (ΔZ) in which charge-blobs are generated due to a gamma-ray event (a) or beta-ray event (b), and are contained only in one segmented drift region.